Energy Conversion and Management 65 (2013) 564–573

Contents lists available at SciVerse ScienceDirect

Energy Conversion and Management

journal homepage: www.elsevier.com/locate/enconman

Reactivity of dolomite in water-saturated supercritical carbon dioxide: Significance for carbon capture and storage and for enhanced oil and gas recovery

Xiuyu Wang [a,1], Vladimir Alvarado [b], Norbert Swoboda-Colberg [a], John P. Kaszuba [a,c,*]

[a] Department of Geology and Geophysics, 1000 E. University Avenue, University of Wyoming, Laramie, WY 82071, USA
[b] Department of Chemical and Petroleum Engineering, 1000 E. University Avenue, University of Wyoming, Laramie, WY 82071, USA
[c] School of Energy Resources, 1000 E. University Avenue, University of Wyoming, Laramie, WY 82071, USA

ARTICLE INFO

Article history:
Received 17 December 2011
Received in revised form 18 July 2012
Accepted 26 July 2012
Available online 5 November 2012

Keywords:
Carbon capture and storage
Enhanced oil recovery
Enhanced gas recovery
Fluid–rock interactions
Supercritical carbon dioxide
Mineralization

ABSTRACT

Carbon dioxide injection in porous reservoirs is the basis for carbon capture and storage, enhanced oil and gas recovery. Injected carbon dioxide is stored at multiple scales in porous media, from the pore-level as a residual phase to large scales as macroscopic accumulations by the injection site, under the caprock and at reservoir internal capillary pressure barriers. These carbon dioxide saturation zones create regions across which the full spectrum of mutual CO_2–H_2O solubility may occur. Most studies assume that geochemical reaction is restricted to rocks and carbon dioxide-saturated formation waters, but this paradigm ignores injection of anhydrous carbon dioxide against brine and water-alternating-gas flooding for enhanced oil recovery.

A series of laboratory experiments was performed to evaluate the reactivity of the common reservoir mineral dolomite with water-saturated supercritical carbon dioxide. Experiments were conducted at reservoir conditions (55 and 110 °C, 25 MPa) and elevated temperature (220 °C, 25 MPa) for approximately 96 and 164 h (4 and 7 days). Dolomite dissolves and new carbonate mineral precipitates by reaction with water-saturated supercritical carbon dioxide. Dolomite does not react with anhydrous supercritical carbon dioxide. Temperature and reaction time control the composition, morphology, and extent of formation of new carbonate minerals.

Mineral dissolution and re-precipitation due to reaction with water-saturated carbon dioxide may affect the contact line between phases, the carbon dioxide contact angle, and the relative permeability and permeability distribution of the reservoir. These changes influence fundamental properties of hysteresis of drainage and imbibition cycles, rock wettability, and capillary pressure. The efficacy of physical carbon dioxide trapping mechanisms, integrity of caprock, and injectivity of a carbon dioxide storage reservoir as well as the injectivity and production rate of an enhanced oil recovery operation may be affected.

1. Introduction

The importance of Carbon Capture and Storage (CCS) to mitigating greenhouse emissions is well established [1–9]. Deep saline formations [1] and depleted oil and gas reservoirs [10–13] are leading targets for carbon dioxide injection and storage (Fig. 1). Injection of carbon dioxide is also used to enhance oil or gas recovery (CO_2-EOR or CO_2-EGR) in hydrocarbon reservoirs (Fig. 2).

Four trapping and storage mechanisms are widely discussed in the CCS literature: structural, residual (also known as capillary trapping), hydrodynamic and mineral trapping [14]. Carbon dioxide can become a residual phase in two- and three-phase flow due to capillary action. As carbon dioxide is injected into a reservoir, anhydrous or "dry" carbon dioxide moves through the porous media and displaces resident fluids as a non-wetting phase. Capillary effects such as snap-off [15] can leave some of the carbon dioxide behind as disconnected droplets. In addition, internal heterogeneities in the formation can trap carbon dioxide at saturations well above its residual value [16,17]. Water drainage and rewetting (or imbibition) are impacted by the advancing and receding contact angles, respectively, which contribute to multiphase flow hysteresis [18]. This hysteresis plays a very important role in residual trapping [16–19]. In the absence of significant hysteresis, little capillary trapping occurs, but local capillary trapping offers a mechanism for high saturation of carbon dioxide in the reservoir [16,20].

* Corresponding author at: Department of Geology and Geophysics, 1000 E. University Avenue, University of Wyoming, Laramie, WY 82071, USA. Tel.: +1 307 766 6065; fax: +1 307 766 6679.
E-mail address: John.Kaszuba@uwyo.edu (J.P. Kaszuba).
[1] Present address: Petroleum Engineering Department, China University of Petroleum-Beijing, 18 Fuxue Rd., Changping District, Beijing 102249, China.

0196-8904/$ - see front matter © 2012 Elsevier Ltd. All rights reserved.
http://dx.doi.org/10.1016/j.enconman.2012.07.024

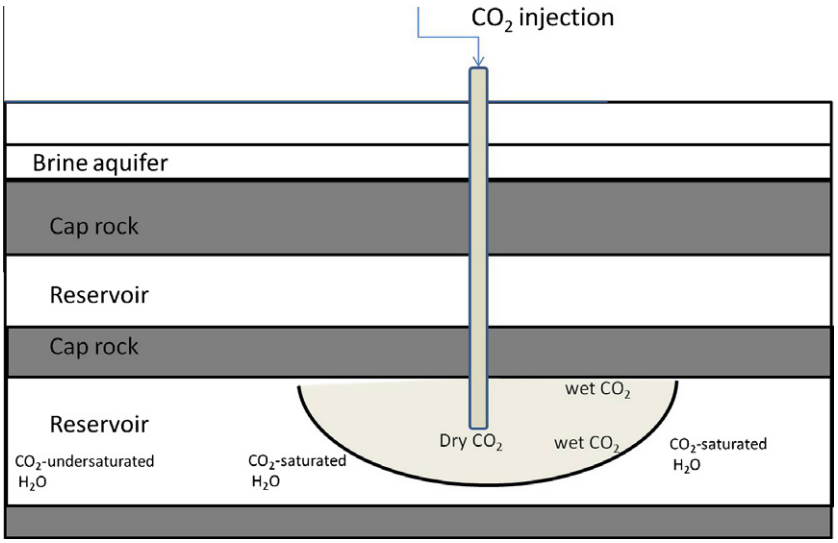

Fig. 1. Schematic diagram of CCS scenario in a saline aquifer. Injection of carbon dioxide creates regions across which the full spectrum of mutual CO_2–H_2O solubility may occur. Anhydrous supercritical carbon dioxide occurs at the injection well; CO_2-saturated and -undersaturated formation waters occur at the displacement front. H_2O-saturated and -undersaturated or "wet" supercritical carbon dioxide can exist between these two extremes, toward the cap rock and at the CO_2–H_2O front.

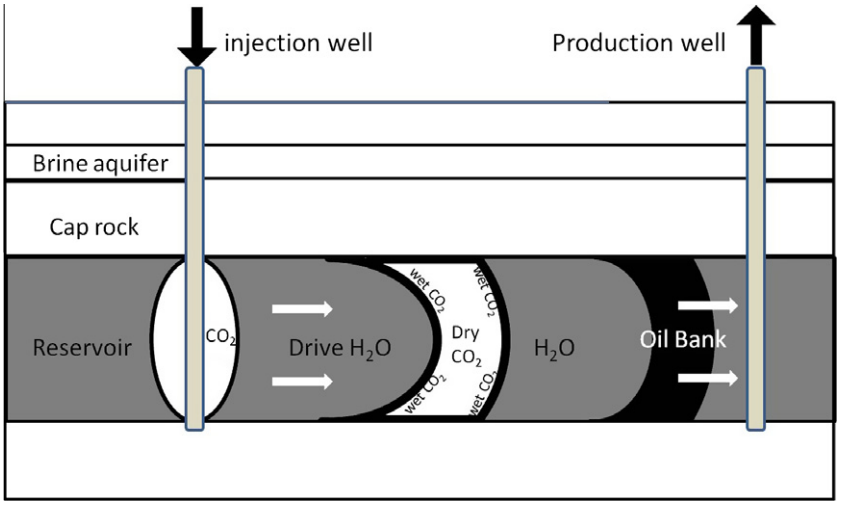

Fig. 2. Schematic diagram of CO_2 injection and enhance oil recovery (modified from http://www.fe.doe.gov/programs/oilgas/eor/). As described in Fig. 1, injection of carbon dioxide creates regions across which the full spectrum of mutual CO_2–H_2O solubility may occur (Figs. 1 and 2). This is only schematic and does not show the mixing zone between carbon dioxide and water. In reality, gravitational ascension of carbon dioxide and water slumping will take place as the mixing zone between fluids destabilizes. The successive fluid slugs create multiphase flow hysteresis that traps both water and carbon dioxide, leading to formation of oil banks and enhanced recovery.

During the injection period in CCS (and similarly in CO_2-EOR), water (or hydrocarbon) displacement is piston-like, mostly controlled by viscous forces. This creates a near-wellbore region, on the order of several meters [15,21], where dry-out occurs. Deeper into the formation, or in post-injection scenarios, carbon dioxide rises due to buoyancy. The saturation distribution of carbon dioxide transitions from the desiccation or dryout zones in the near-wellbore area, a few meters from the injection site, to trapped carbon dioxide. Thus, carbon dioxide injection creates regions across which the full spectrum of mutual CO_2–H_2O solubility may occur (Fig. 1). Dry supercritical carbon dioxide exists at the injection-well nearby area, as a result of dry-out, whereas CO_2-saturated and -undersaturated formation waters exist at the displacement front. H_2O-saturated and -undersaturated or "wet" supercritical carbon dioxide can exist between these two chemical extremes, toward the cap rock due to buoyancy forces [15,16] and at the CO_2–H_2O front.

Carbon dioxide can act as a wetting fluid [18] potentially leading to mixed-wettability [22]. In this scenario, different mineral surfaces are exposed to different fluids, namely either water or CO_2. The reactivity of carbon dioxide with mineral surfaces will depend on its distribution in the pore space. In contrast, most geochemical and reservoir models assume mineral surface reactivity with carbonic acid [e.g., 23,24]. Experimental laboratory studies that evaluate fluid–rock and fluid–mineral interactions relevant to CCS and EOR scenarios traditionally focus on reactions among minerals and aqueous solutions [e.g., 25–29]. These studies are performed at conditions corresponding to CO_2-saturated and -undersaturated formation waters at the displacement front. More recently, experimental studies have begun to evaluate the reactivity of silicate and hydroxide minerals with wet supercritical carbon dioxide [30–40]. These studies agree that silicate and hydroxide minerals react with wet supercritical carbon dioxide and form carbonate minerals. Regnault et al. [41] also evaluated the reactivity

of portlandite and dolomite with wet supercritical carbon dioxide but only reported results for portlandite. Not surprisingly, portlandite is highly reactive with wet supercritical carbon dioxide. Clearly it is important to understand the interactions take place between rocks and wet supercritical carbon dioxide in CCS, CO_2-EOR, and CO_2-EGR reservoirs.

In this paper we investigate the reactivity of the mineral dolomite with wet (H_2O-saturated) supercritical carbon dioxide in laboratory experiments. We selected dolomite because it is a common rock-forming mineral in carbonate reservoirs as well as carbonate-bearing siliciclastic reservoirs targeted for CCS, CO_2-EOR, and CO_2-EGR. Laboratory experiments were performed at 55 and 110 °C, temperatures characteristic of reservoir conditions such as those found in Southwest Wyoming. We also performed experiments at 220 °C to accelerate reaction rates and enhance the likelihood for results at realistic laboratory time scales. Our study qualitatively evaluates dolomite reactivity in H_2O-saturated carbon dioxide; quantitative assessment of reaction mechanisms and kinetics are beyond the scope of this study. This study demonstrates that dolomite is reactive in H_2O-saturated supercritical carbon dioxide and explores implications for this reactivity with respect to CCS, CO_2-EOR, and CO_2-EGR in carbonate-bearing formations and hydrocarbon reservoirs.

2. Experimental methods

2.1. Approach and design

Our approach was to conduct experiments that react dolomite with H_2O-saturated supercritical carbon dioxide (Fig. 3). Recent experimental work demonstrates mineral reactivity with H_2O-undersaturated supercritical carbon dioxide [30–40]; thus dolomite reactivity in H_2O-undersaturated supercritical carbon dioxide presents a potentially fruitful avenue of investigation. However, evaluating these complexities will require additional experiments and is beyond the scope of this investigation. Therefore, for this study, maintaining water saturation was a key aspect. Water is consumed if, for example, carbonate minerals such as nesquehonite, dypingite, and hydromagnesite precipitate. To ensure water saturation of supercritical carbon dioxide for the duration of each experiment we added de-ionized water to the bottom of the reaction chamber in an amount greater than needed for saturation (Table 1). The mass of water needed to saturate supercritical carbon dioxide at the temperature and pressure conditions of each experiment was determined using equations of state for carbon dioxide [42].

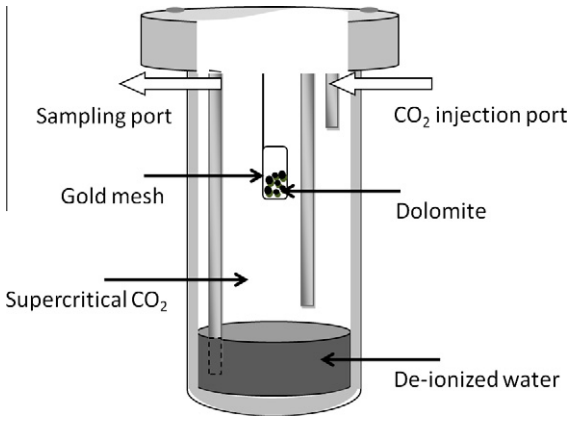

Fig. 3. Schematic diagram of experimental apparatus and design. The reaction chamber is a 300-cm^3 customized bolted closure reactor manufactured by Autoclave Engineers. The reaction chamber and its multiple tubing inlets and outlets are constructed of Hastelloy C-276.

The presence of liquid water in the reaction chamber presents the possibility of dolomite reaction as an artifact of the experimental procedure. Splashing water onto the dolomite, for example, could take place while injecting carbon dioxide. Our design and procedures (Section 2.3) were implemented to ensure that dolomite and bulk water remained physically separated during the experiment. As one check on our methods, one experiment was repeated using an alternative method of introducing water into the reaction chamber. As a second check on our methods, aqueous samples were withdrawn from each ongoing experiment and after terminating each experiment. This method check assumes that the chemistry of the water sampled from the bottom of the reactor will change if water splashes onto and drains from the dolomite during the course of the experiment or if dolomite powders are washed off of dolomite fragments and into the water reservoir. Thus our design provides sufficient water in the bottom of the reactor for sampling purposes while simultaneously minimizing the amount of water to avoid splashing it onto the dolomite.

2.2. Apparatus and materials

The experimental apparatus consists of a pressurized reaction chamber and furnace (Fig. 3). The experimental design places de-ionized water in the bottom of the reaction chamber and supercritical carbon dioxide with a grade of 99.95% in the top. A sample holder constructed of gold mesh and wire secures the sample above the water and in the carbon dioxide. The mesh is 99.9% pure gold and possesses a nominal aperture of 0.25 mm.

Research grade dolomite ($CaMg(CO_3)_2$) was purchased from Ward Scientific (#49V 1557, Selasvann, Norway). The mineral composition was determined by inductively coupled plasma optical emission spectrometer (ICP-OES) after digestion with hydrochloric acid. The ratio of calcium to magnesium is about 1.3 and the ratio of magnesium to iron ranges from 4.4 to 4.5 (Fig. 4). The dolomite is not uniform in composition because it contains veinlets of calcite. Use of heterogeneous dolomite does not allow us to determine quantitative reaction parameters for these experiments but does approximate natural field conditions more closely.

Dolomite was prepared for the experiments in two different ways. In the first method, dolomite fragments were stored in a container and permitted to accumulate dolomite powder on mineral surfaces due to abrasion among the fragments. The advantage of this method is that dolomite reactive surface area and the resulting kinetic rates increase, enhancing reactivity at laboratory time scales. The disadvantages are that we do not have rigorous control on the distribution of the powders on mineral surfaces and that we cannot quantify the reactive surface area of the powders. Another disadvantage is that the mineralogy of the powders varies because, as described in the previous paragraph, their dolomite source is not homogeneous. All but one of the experiments was conducted using dolomite prepared in this manner. In the alternate preparation method, dolomite was cleansed of all powders. To accomplish this, dolomite fragments were rinsed with and sonicated in de-ionized water for 30 min, rinsed with de-ionized water three times, rinsed with methanol, dried overnight in a hood, and dried overnight in an oven at 110 °C. This method allows us to evaluate whether the use of mineral powders induced artifacts into our experiments. SEM images of dolomite prepared using these methods are presented in Fig. 5.

2.3. Procedures

De-ionized water was first placed at the bottom of the reaction vessel (Fig. 3). The gold mesh containing 1 g of dolomite fragments

Table 1
Summary for the experiments performed and major cation analysis of water samples (in millimole/kg).

#	T (°C)	Information regarding H_2O	Dolomite starting material	Time (h)	X_{H_2O} in reactor at beginning of experiment	pH[a]	Ca	Mn	Fe	Mg	Na	Comment
		De-ionized H_2O	–			6.8	0.2155	0.0002	0.0002	0.1198	0.0873	Composition of H_2O added to reactor
1	110	Anhydrous CO_2	Fragments + powder	272	0	–	–	–	–	–	–	Control experiment
2	55	H_2O added before reactor is sealed (standard method)	Fragments + powder	93	0.24	4.9	0.1339	0.0006	0.0064	0.0596	0.1014	–
3	220	H_2O added by standard method	Fragments + powder	94	0.49	4.4	0.5888	0.0129	0.0122	0.0271	0.1048	–
4	220	H_2O injected after reactor is sealed	Fragments + powder	90	0.5	4.2	NA[b]	NA	NA	NA	NA	–
5	55	H_2O added by standard method	Fragments + powder	164	0.24	4.7	0.1137	0.0043	0.0154	0.0668	0.0619	–
6	220	H_2O added by standard method	Fragments + powder	162	0.44	4.7	0.0097	0.0009	<0.00013	<0.00052	<0.00147	–
7	220	H_2O added by standard method	Fragments, no powder	94	0.48	4.6	0.067	0.0043	0.0012	<0.00157	0.2103	Sonicate dolomite 30 min

[a] pH measured on samples cooled to 25 °C and depressurized to 0.1 MPa.
[b] Not available, sample container leaked.

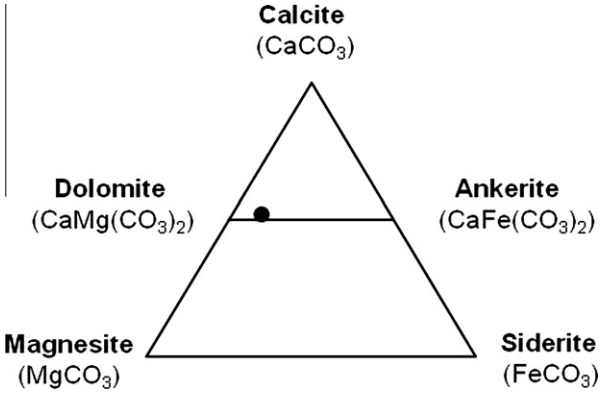

Fig. 4. Ternary diagram illustrating composition of dolomite (in mole%) used in the experiments.

(approximately 3 mm in diameter) was emplaced and the reactor sealed. To avoid generating steam that could have reacted with dolomite, the reactor was pressurized to about 5 MPa before heating. Pressurization was accomplished by injecting carbon dioxide through the port at the top of the reactor (Fig. 3) using a syringe pump at a low flow rate (5 ml/min). The reactor was subsequently heated to the predetermined temperature of the experiment. Carbon dioxide was again injected until the final pressure of 25 MPa was reached.

To evaluate our procedures, one experiment was performed using a different method of adding water into the reaction chamber. In this experiment (Experiment #4 Table 1), dolomite was sealed in the reactor without water. Carbon dioxide was injected to a pressure of 5 MPa, then water was injected at a flow rate of 5 ml/min into the bottom of the reactor through the sampling tube (Fig. 3). The furnace was subsequently heated to 220 °C. Additional carbon dioxide was then injected until the pressure reached 25 MPa.

The mass of water placed in the reactor at the beginning of each experiment ranged from 23 to 37 g. The mole fraction of water relative to carbon dioxide in the reactor at the beginning of the experiment was equal to or less than 0.5 (Table 1). The temperature of

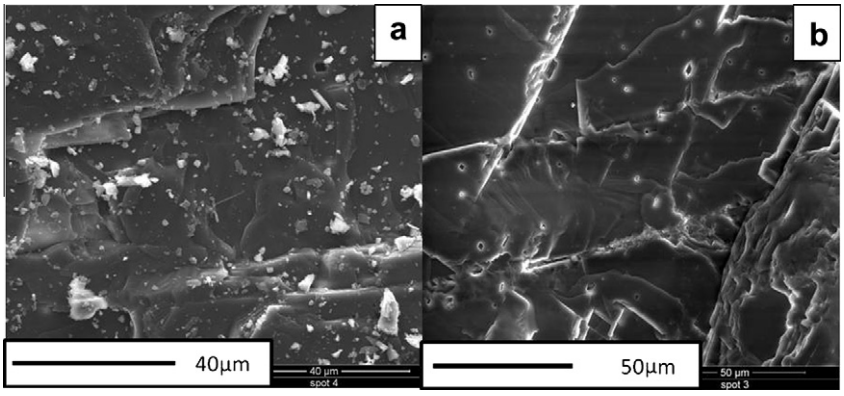

Fig. 5. Secondary electron SEM micrographs of unreacted dolomite. (a) Dolomite fragments containing dolomite powder on mineral surfaces. (b) Dolomite cleansed of mineral powders.

each experiment was maintained to within 0.2 °C and the pressure to within 0.7 MPa.

Aqueous samples were withdrawn from ongoing experiments using the sampling tube that extends to the deepest portion of the reactor (Fig. 3). About 1 ml of solution was first collected and discarded to rinse the sampling tube and fill it with fresh fluid. The pH was subsequently determined on samples cooled to 25 °C and depressurized to 0.1 MPa using a Thermo Scientific Orion 4 Star pH meter and Ross micro electrode. Samples for cation analysis were filtered using a 0.45 μm filter and diluted 10×. To prevent mineral precipitation, the samples for cation analysis were acidified to pH 2 using trace metal grade nitric acid and stored at about 5 °C prior to analysis. Cations were analyzed with an ARL 3410+ ICP-OES. Mineral precipitants were not observed in any of the fluid samples. At the conclusion of each experiment the reacted dolomite was recovered, weighed, and dried in air prior to analysis. Recovered minerals were analyzed using optical microscopy, scanning electron microscopy (SEM), and energy dispersive spectra (EDS). Mineral growth in the experiments was insufficient for analysis by X-ray diffraction (XRD) or electron probe microanalysis (EPMA).

3. Results

Experiments reacting dolomite with H_2O-saturated supercritical carbon dioxide were performed at 25 MPa, 55 °C and 220 °C for approximately 96 and 164 h (approximately 4 and 7 days) (Table 1). A control experiment that reacted dolomite with anhydrous supercritical carbon dioxide for 272 h (Experiment #1) was performed at an intermediate temperature of 110 °C. Dolomite fragments containing dolomite powder on mineral surfaces were used in this experiment. No evidence of dolomite dissolution or mineral growth was observed in this experiment (Fig. 6).

SEM and EDS analysis of dolomite reacted with H_2O-saturated supercritical carbon dioxide at 55 °C for 93 and 164 h (Experiments #2 and #5, respectively) are shown in Fig. 7. Dolomite fragments containing dolomite powder on mineral surfaces were used in these two experiments. At the conclusion of both experiments, dolomite fragments exhibit edges of cleavage planes that are no longer straight and smooth but are rounded and rough due to dissolution. Dolomite powders are no longer present on mineral surfaces. A new carbonate mineral exhibiting irregular morphology precipitated on dolomite surfaces. Crystals of this morphology are not present on unreacted dolomite (Fig. 5a) or on the dolomite reacted with anhydrous supercritical carbon dioxide (Fig. 6a). EDS spectra suggest that this carbonate mineral contains magnesium, calcium, and iron in relative proportions consistent with dolomite. Iron may be more abundant compared to the unreacted dolomite, however, the EDS spectra are not conclusive. New mineral growth covers a larger area of the dolomite in the 164-h experiment compared to the 93-h experiment. The absence of quench morphology of the new crystals and the greater extent of mineral growth as a function of reaction time suggest that mineral growth took place during the experiment and is not an artifact of the quenching process.

The results of SEM and EDS analysis of dolomite reacted with H_2O-saturated supercritical carbon dioxide at 220 °C for 94 and 162 h (Experiments #3 and #6, respectively) are shown in Fig. 8. Dolomite fragments containing dolomite powder on mineral surfaces were also used in these two experiments. Dolomite powders are no longer present on mineral surfaces at the conclusion of both experiments. Two new minerals grew on dolomite surfaces, one exhibiting platelet morphology and a second of rhombohedral carbonate crystals (Fig. 8). Crystals exhibiting these morphologies are not present on unreacted dolomite (Fig. 5a) or on the dolomite reacted with anhydrous supercritical carbon dioxide (Fig. 6a). The rhombohedral carbonates are euhedral crystals ranging in size from 1 to 5 or more microns. EDS spectra suggest that these rhombohedral carbonate minerals contain magnesium, calcium, and iron in relative proportions consistent with dolomite. Iron may again be more abundant compared to the original dolomite, however the EDS spectra are not conclusive.

An additional experiment reacted dolomite with H_2O-saturated supercritical carbon dioxide at 220 °C for 90 h (Experiment #4). This is the experiment in which water was introduced into the reaction chamber by an alternate method (Section 2.3). Dolomite fragments containing dolomite powder on mineral surfaces were also used in this experiment. Dolomite powders are no longer present on mineral surfaces at the conclusion of both experiments. Two new minerals grew on dolomite surfaces, one exhibiting platelet morphology and a second of rhombohedral carbonate crystals. These are the same morphologies as observed in experiments performed at 220 °C with water sealed in the bottom of the reaction chamber at the beginning of the experiment (Experiments #3 and #6, compare Fig. 8a–c and g–i). The growth of crystals with similar morphology in these experiments provides confidence that the liquid water reservoir remains physically separated from the dolomite during the experiment.

Dolomite fragments cleansed of mineral powders (Section 2.1) reacted with H_2O-saturated supercritical carbon dioxide at 220 °C in one experiment (Experiment #7). Cleavage planes became more abundant and prominent in dolomite fragments (compare Fig. 5a and b). Two new minerals grew on dolomite surfaces. Newly-formed rhombohedral carbonate crystals range from a submicron

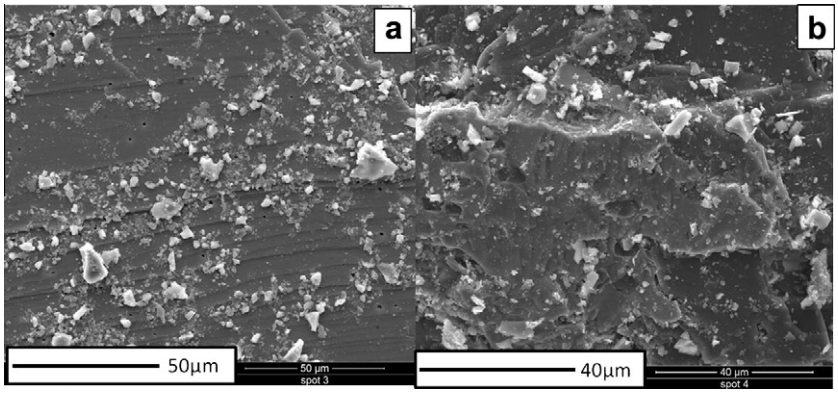

Fig. 6. Secondary electron SEM micrographs of (a) dolomite after reaction with anhydrous carbon dioxide at 110 °C and 272 h. No evidence of dolomite dissolution or mineral growth was observed in this experiment. (b) Unreacted dolomite.

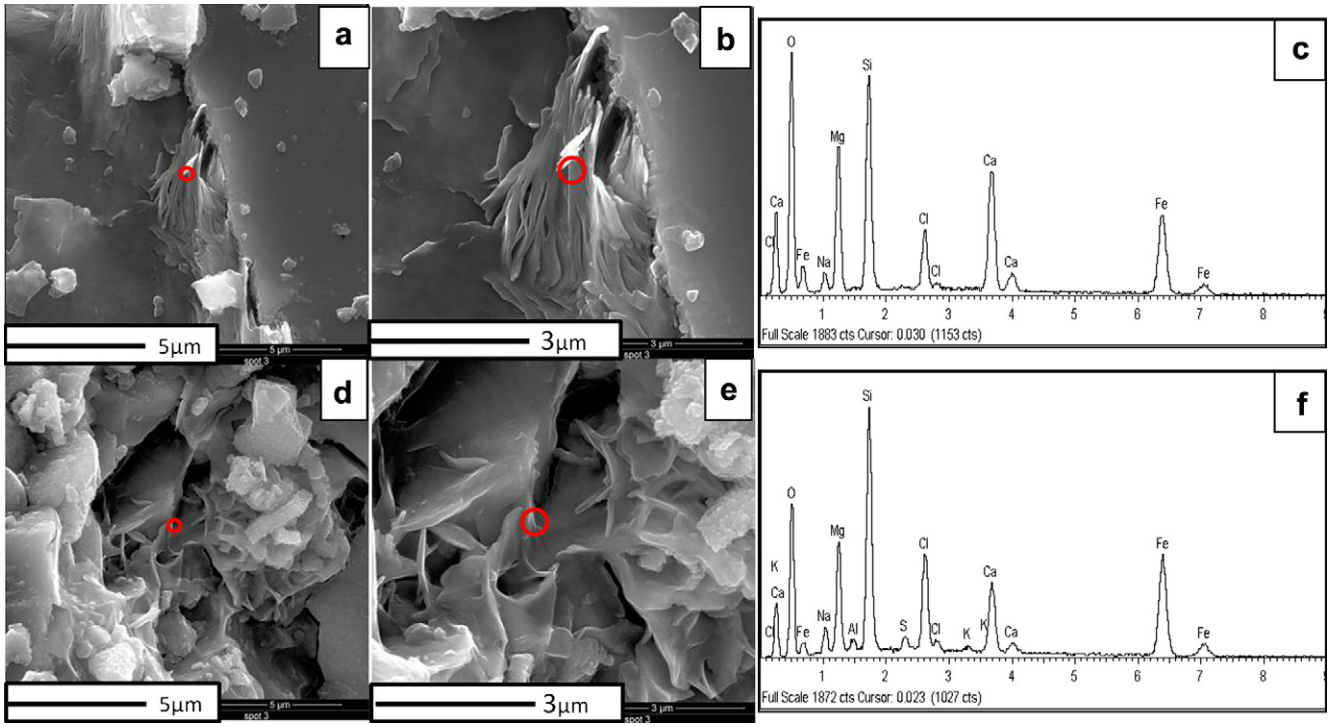

Fig. 7. Secondary electron SEM micrographs and EDS spectra of dolomite reacted with H_2O-saturated supercritical carbon dioxide at 55 °C. Dolomite used in these experiments contained powder on mineral surfaces. (a–c) Reaction for 93 h (Experiment #2 in Table 1). (d–f) Reaction for 164 h (Experiment #5 in Table 1). New mineral growth exhibiting irregular morphology is observed. EDS spectra are consistent with this mineral being recrystallized dolomite. New mineral growth covers a larger area of the dolomite in the 164-h experiment compared to the 93-h experiment.

scale to 1–3 μm in size (Fig. 10). Submicron platelets of new crystal growth are also evident (Fig. 9a and b), but the crystals could not be identified by morphology or by EDS spectra. Neither morphology is present on unreacted dolomite (Figs. 5b) or on the dolomite reacted with anhydrous supercritical carbon dioxide (Fig. 6a). New crystal growth covers a much larger proportion of mineral surfaces compared to experiments that reacted dolomite fragments containing dolomite powder on mineral surfaces. EDS spectra collected from the large rhombohedral carbonates suggests that these crystals may contain more iron compared to the unreacted dolomite.

The analytical results reported in Table 1 are for aqueous samples collected immediately prior to terminating each experiment. We do not report bicarbonate analyses because the immiscible supercritical carbon dioxide present throughout the experiment maintains carbon dioxide saturation in the water. Except for pH, the de-ionized water analysis and the analysis of the water samples collected from each experiment are similar. These relationships suggest that dolomite and bulk water did not directly interact with each other and that dolomite powder was not washed off of dolomite fragments during the experiments. In fact, several experiments were rejected because water sampled from these experiments contained elevated cation concentrations relative to the de-ionized water used in the reaction chamber, indicating that dolomite and water had interacted with each other.

4. Discussion

Computer simulations of carbon dioxide storage in deep saline aquifers focus on trapping mechanisms and processes involving the reservoir and CO_2-saturated formation waters [e.g., 15–17,21]. Studies such as these implicitly assume that all reactions take place in the water–rock environment or conclude that injected carbon dioxide does not react directly with minerals. Our results demonstrate that chemical reaction takes place between dolomite and H_2O-saturated supercritical carbon dioxide. Dolomite fragments exhibit dissolution textures and dolomite powders are no longer present on mineral surfaces. A new carbonate mineral precipitated in the experiments performed at reservoir temperatures (55–110 °C); this mineral growth covers a larger area in a longer-running experiment. Experiments performed at higher temperatures of 220 °C produced both platelets and rhombohedral carbonates. New crystal growth covered an even larger proportion of mineral surfaces of dolomite cleansed of powders, likely due to relaxation of the lattice strain produced by the cleaning process. No net mineralization occurred in these experiments because cations provided for carbonate precipitation can only be derived from dissolution of the original dolomite. However, the fact that reaction even takes place between dolomite and carbon dioxide suggests that regions within CCS, CO_2-EOR, and CO_2-EGR reservoirs that are believed to be non-reactive are in fact susceptible to chemical reaction.

Our findings are consistent with recent studies that have determined that silicate and hydroxide minerals react with wet supercritical carbon dioxide [30–40]. A thin film of water (a few nanometer thick) develops on the surface of minerals in contact with H_2O-undersaturated as well as H_2O-saturated supercritical carbon dioxide [33,35]. In addition, dolomite has been found to exhibit hydrophilic surfaces [43] under mixed [44] or oil wet [45] conditions. Water composition [46,47] and temperature [45] can turn oil-wet carbonate into a more hydrophilic surface. Oil wettability is usually associated with the presence of organic material in the depositional environment [44]. Despite the overall neutral or oil wet condition, dolomite often contains water-wet surfaces. Hydrophilic surfaces always develop a precursor nanoscale wetting film ahead of the contact line. Surface roughness offers capillary traps that enhance the formation of liquid films that can be at equi-

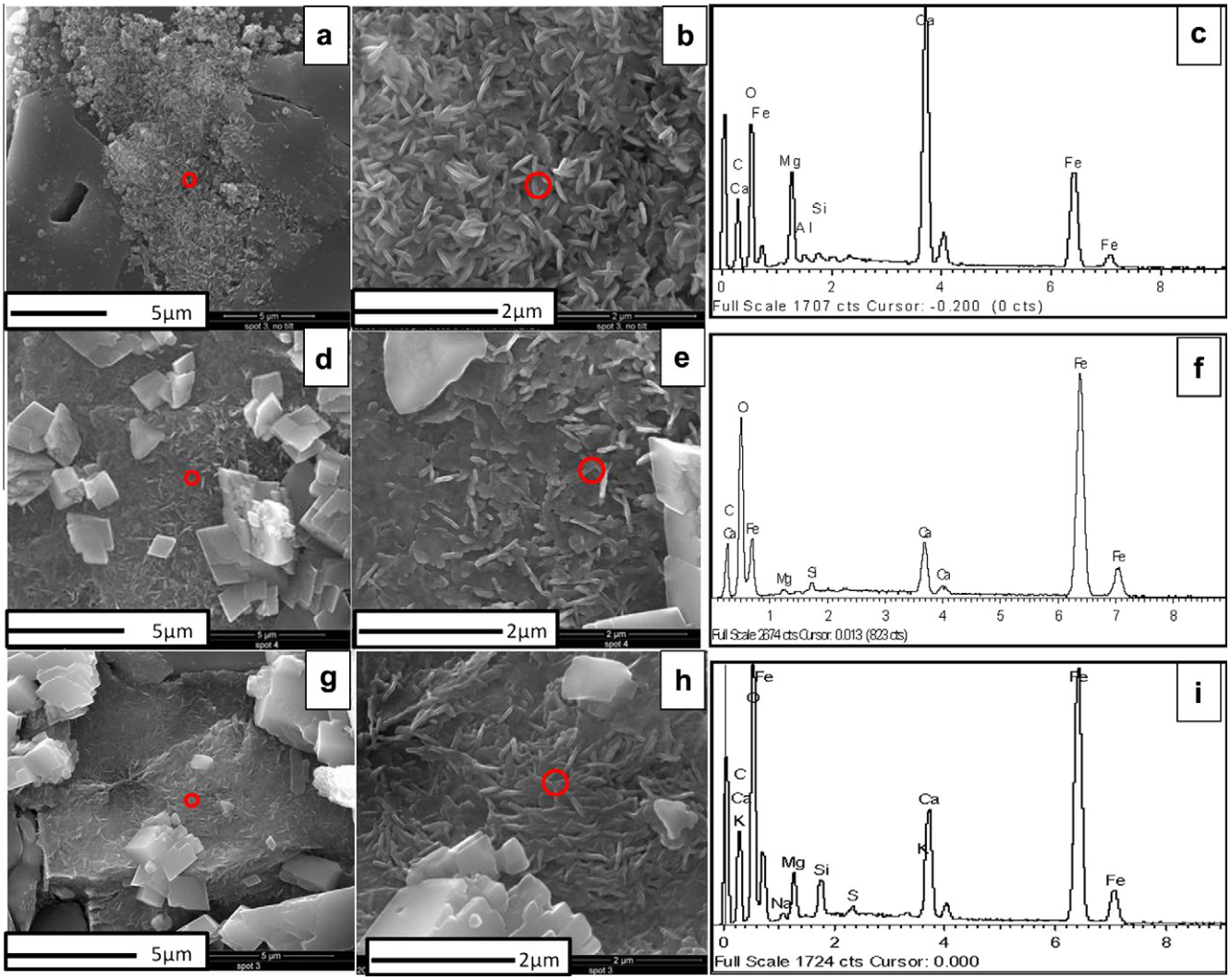

Fig. 8. Secondary electron SEM micrographs and EDS spectra of dolomite reacted with H_2O-saturated supercritical carbon dioxide at 220 °C. Dolomite used in these experiments contained powder on mineral surfaces. (a–c) Reaction for 94 h, standard method of adding de-ionized water to the bottom of the reaction chamber before sealing the reactor was employed (Experiment #3 in Table 1). (d–f) Reaction for 162 h, de-ionized water added by standard method (Experiment #6 in Table 1). (g–i) Reaction for 90 h, de-ionized water added to bottom of reactor after sealing the reactor (Experiment #4 in Table 1). Two types of new mineral growth are observed, one exhibiting platelet morphology and a second of rhombohedral carbonate crystals. EDS spectra of rhombohedral carbonate minerals are consistent with recrystallized dolomite. Iron may be more abundant compared to unreacted dolomite, however the EDS spectra are not conclusive. Rhombohedral carbonate crystals depicted in (g) and (h) are out of the field of view in (a) and (b).

librium with saturated phases [48]. In this sense, we expected the existence of water films on dolomite in our experiments. We speculate that these films can lead to new mineral growth. However, we currently lack the molecular-scale data needed to conclusively make this determination.

Our findings are also consistent with recent studies that have determined the reactivity of minerals with anhydrous supercritical carbon dioxide. In one study, montmorillinite loses interlayer water when exposed to anhydrous supercritical carbon dioxide, depending on the initial hydration state of the clay [39]. In a second pair of studies, montmorillinite expands due to carbon dioxide migration into the interlayer [34,38]. In contrast, anhydrous supercritical carbon dioxide does not react with minerals that lack the expandable/collapsible interlayer spacing of swelling clays, including forsterite [32,33,35], kaolinite [34], brucite [36,40], and, as we demonstrate, dolomite.

The reaction of minerals and wet supercritical carbon dioxide potentially holds several implications for CCS, CO_2-EOR, and CO_2-EGR fluid–rock systems. Mineral dissolution and re-precipitation may redistribute the porous matrix of the reservoir. This process can impact multi-phase flow of the reservoir by changing the dynamics of the contact line between phases and, therefore, changing hysteresis of drainage and imbibition cycles. Previous modeling results show weak hysteresis effects or changes of relative permeability [49]. However, the experimental conditions that were simulated neglect the impact of wet carbon dioxide reacting with mineral surfaces. Since the carbon dioxide saturation distribution arises from multiscale phenomena and a multitude of reactive conditions, wettability alteration as well as surface roughness may vary significantly between surfaces reacted with CO_2-saturated formation waters and those reacted with wet carbon dioxide. New growth on mineral surfaces may also change the carbon dioxide contact angle, consequently altering wettability of rock and capillary pressure, which in turn can affect physical carbon dioxide trapping mechanisms. Wettability alteration, leading to lower water wettability in clastic rocks, has been demonstrated through

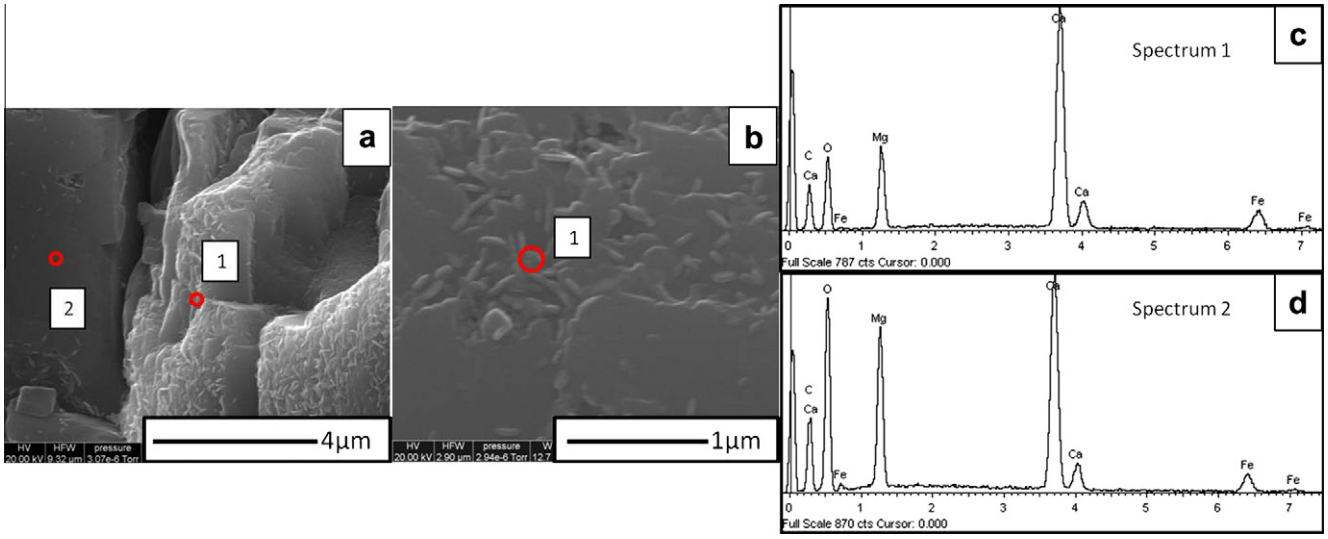

Fig. 9. Secondary electron SEM micrographs and EDS spectra of dolomite reacted with H_2O-saturated supercritical carbon dioxide at 220 °C. Dolomite used in this experiment was cleansed of mineral powders. Two types of new mineral growth are observed, submicron scale platelets (a and b) and submicron scale rhombohedral carbonate crystals (not pictured). New crystal growth in this experiment covers a much larger proportion of mineral surfaces compared to experiments that reacted dolomite containing dolomite powder on mineral surfaces.

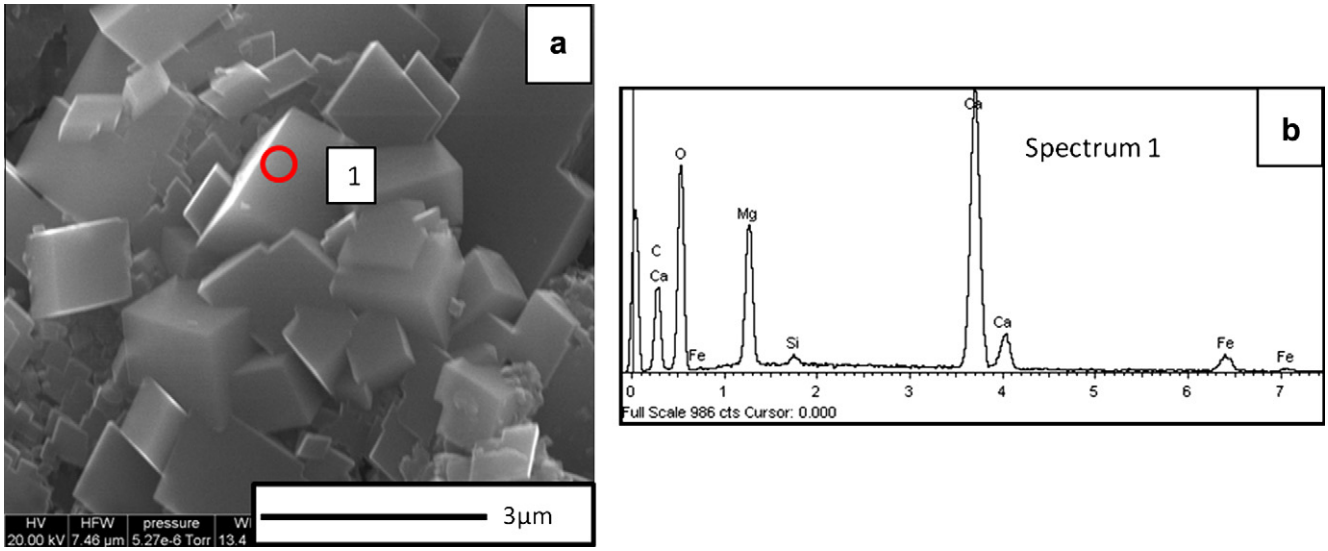

Fig. 10. Secondary electron SEM micrographs and EDS spectra of dolomite reacted with H_2O-saturated supercritical carbon dioxide at 220 °C. Dolomite used in this experiment was cleansed of mineral powders. (a) Dolomite rhombohedrons. (b) EDS spectra of point 1 in (a) is consistent with this mineral being recrystallized dolomite.

contact angle measurements [50,51]. This process is particularly important for the ability of the caprock to act as barrier against carbon dioxide migration.

In CO_2-EOR and CO_2-EGR, reaction of carbonate rock with wet supercritical carbon dioxide may affect the three-phase mixing zone and the efficiency of the recovery process. This may occur by modifying phase mobility through changes in relative permeability [52]. Reaction of carbonate rock with wet supercritical carbon dioxide may possibly change the permeability of the reservoir by redistributing minerals, if precipitation–dissolution events occur at pore throats. These events will be regulated by the state of saturation of carbon dioxide as it displaces brine or in regions highly saturated with carbon dioxide, as well as by the mutual solubility of phases and capillary pressure. Since carbon dioxide acts as a good solvent for crude oil, regions of very low oil saturation are possible and the interplay of wettability alteration and multiphase flow hysteresis can lead to regions of high carbon dioxide saturation, even in cases of three-phase flow displacement. We speculate that mixed wettability can be significantly affected by drying of water-wet films and direct contact of surfaces by water-loaded carbon dioxide. The change of permeability, as well as capillary pressure and relative permeability, will affect the injection rate (injectivity) and oil production rate during CO_2-EOR. Carbon dioxide can also become more mobile in a CCS reservoir as the result of wettability alteration, thus affecting carbon dioxide storage capacity in these reservoirs.

Reaction with wet supercritical carbon dioxide may also affect the caprocks that seal CCS, CO_2-EOR, and CO_2-EGR reservoirs. Mineral reactions in the caprock that produce negative volume changes may yield zone of higher permeability and subsequent release of carbon dioxide. Alternatively, mineral reactions producing positive volume changes may lead to reduced porosity and permeability and enhance the sealing characteristics of the caprock. Both of these scenarios illustrate the richness of geochemical complex-

ity previously unexamined. Secure storage of carbon dioxide in a CCS, CO_2-EOR, or CO_2-EGR scenario must account for these potential reactions.

5. Conclusions

The reactivity of dolomite with H_2O-saturated supercritical carbon dioxide was studied at reservoir conditions (55–110 °C, 25 MPa) and elevated temperature (220 °C, 25 MPa) for reaction times of approximately 96 and 164 h (approximately 4 days and 7 days). Dolomite does not react with anhydrous supercritical carbon dioxide. Dolomite dissolves and carbonate minerals precipitate by reaction with H_2O-saturated supercritical carbon dioxide. Temperature and reaction time control the composition, morphology, and extent of formation of new carbonate minerals. Crystals with irregular morphology precipitate at 55 °C; crystal platelets and rhombohedral dolomite precipitate at 220 °C.

Mineral dissolution and re-precipitation due to reaction with H_2O-saturated supercritical carbon dioxide may affect the dynamics of the contact line between phases, the carbon dioxide contact angle, and the relative permeability and permeability distribution of the reservoir. Changes to these fundamental properties may in turn influence hysteresis of drainage and imbibition cycles, wettability of rock, and capillary pressure. On a larger scale, the efficacy of physical carbon dioxide trapping mechanisms, integrity of caprock, and injectivity of a carbon dioxide storage reservoir as well as the injectivity and oil production rate of an EOR operation may be affected.

Acknowledgements

We acknowledge the US Department of Energy for funding through grant DE-FE0002142. John Kaszuba's work was also supported by the UW School of Energy Resources. None of these funding agencies or institutions had a role in the design of the study. We acknowledge The Laboratory for Environmental and Geological Studies (LEGS) at the University of Colorado, particularly Fredrick G. Luiszer, for aqueous analyses. Xiuyu Wang was primarily responsible for the experimental work. Xiuyu Wang and Norbert Swoboda-Colberg performed the SEM work. John Kaszuba and Vladimir Alvarado were responsible for overall mentorship. All four authors shared in manuscript preparation and have approved the final article.

References

[1] Bachu S. Sequestration of CO_2 in geological media: criteria and approach for site selection in response to climate change. Energy Convers Manage 2000;41:953–70.
[2] Gale J, Christensen NP, Cutler A, Torp TA. Demonstrating the potential for geological storage of CO_2: the Sleipner and GESTCO projects. Environ Geosci 2001;8:160–5.
[3] Han WS, McPherson BJ. Optimizing geologic CO_2 sequestration by injection in deep saline formations below oil reservoirs. Energy Convers Manage 2009;50:2570–82.
[4] Gerard D, Wilson EJ. Environmental bonds and the challenge of long-term carbon sequestration. J Environ Manage 2009;90:1097–105.
[5] Voltattorni N, Sciarra A, Caramanna G, Cinti D, Pizzino L, Quattrocchi F. Gas geochemistry of natural analogues for the studies of geological CO_2 sequestration. Appl Geochem 2009;24:1339–46.
[6] Schreiber A, Zapp P, Markewitz P, Vögele S. Environmental analysis of a German strategy for carbon capture and storage of coal power plants. Energy Policy 2010;38:7873–83.
[7] Moore JC, Jevrejeva S, Grinsted A. Efficacy of geoengineering to limit 21st century sea-level rise. Proc Natl Acad Sci USA 2010;107:15699–703.
[8] Yang F, Bai BJ, Tang DZ, Dunn-Norman S, Wronkiewicz D. Characteristics of CO_2 sequestration in saline aquifers. Petrol Sci 2010;7:83–92.
[9] Shukla R, Ranjith P, Haque A, Choi X. A review of studies on CO_2 sequestration and caprock integrity. Fuel 2010;89:2651–64.
[10] Jessen K, Kovscek AR, Orr FM. Increasing CO_2 storage in oil recovery. Energy Convers Manage 2005;46:293–311.
[11] Kovscek AR, Cakici MD. Geologic storage of carbon dioxide and enhanced oil recovery: II. Cooptimization of storage and recovery. Energy Convers Manage 2005;46:1941–56.
[12] Kovscek AR, Wang Y. Geologic storage of carbon dioxide and enhanced oil recovery: I. Uncertainty quantification employing a streamline based proxy for reservoir flow simulation. Energy Convers Manage 2005;46:1920–40.
[13] Zhang YQ, Oldenburg CM, Finsterle S, Bodvarsson GS. System-level modeling for economic evaluation of geological CO_2 storage in gas reservoirs. Energy Convers Manage 2007;48:1827–33.
[14] Bachu S, Gunter WD, Perkins EH. Aquifer disposal of CO_2: hydrodynamic and mineral trapping. Energy Convers Manage 1994;35:269–79.
[15] Pruess K, Muller N. Formation dry-out from CO_2 injection into saline aquifers: 1. Effects of solids precipitation and their mitigation. Water Resour Res 2009;45.
[16] Behzadi H, Alvarado V, Mallick S. CO_2 saturation, distribution and seismic response in two-dimensional permeability model. Environ Sci Technol 2011;45:9435–41.
[17] Krevor SCM, Pini R, Li BX, Benson SM. Capillary heterogeneity trapping of CO_2 in a sandstone rock at reservoir conditions. Geop Res Lett 2011;38.
[18] Pentland CH, El-Maghraby R, Iglauer S, Blunt MJ. Measurements of the capillary trapping of super-critical carbon dioxide in Berea sandstone. Geop Res Lett 2011;38.
[19] Spiteri EJ, Juanes R, Blunt MJ, Orr FM. A new model of trapping and relative permeability hysteresis for all wettability characteristics. SPE J 2008;13:277–88.
[20] Saadatpoor E, Bryant SL, Sepehrnoori K. New trapping mechanism in carbon sequestration. Transp Porous Media 2010;82:3–17.
[21] André L, Audigane P, Azaroual M, Menjoz A. Numerical modeling of fluid–rock chemical interactions at the supercritical CO_2-liquid interface during CO_2 injection into a carbonate reservoir, the Dogger aquifer (Paris Basin, France). Energy Convers Manage 2007;48:1782–97.
[22] Morrow NR, Mason G. Recovery of oil by spontaneous imbibition. Curr Opin Colloid Interface Sci 2001;6:321–37.
[23] Pham VTH, Lu P, Aagaard P, Zhu C, Hellevang H. On the potential of CO_2–water–rock interactions for CO_2 storage using a modified kinetic model. Int J Greenhouse Gas Control 2011;5:1002–15.
[24] Noiriel C, Luquot L, Made B, Raimbault L, Gouze P, van der Lee J. Changes in reactive surface area during limestone dissolution: an experimental and modelling study. Chem Geol 2009;265:160–70.
[25] Kaszuba JP, Janecky DR, Snow MG. Carbon dioxide reaction processes in a model brine aquifer at 200 °C and 200 bars: implications for geologic sequestration of carbon. Appl Geochem 2003;18:1065–80.
[26] Gerdemann SJ, O'Connor WK, Dahlin DC, Penner LR, Rush H. Ex situ aqueous mineral carbonation. Environ Sci Technol 2007;41:2587–93.
[27] Newell DL, Kaszuba JP, Viswanathan HS, Pawar RJ, Carpenter T. Significance of carbonate buffers in natural waters reacting with supercritical CO_2 – implications for monitoring, measuring and verification (MMV) of geologic carbon sequestration. Geop Res Lett 2008;35. http://dx.doi.org/10.1029/2008GL035615.
[28] Garcia B, Beaumont V, Perfetti E, Rouchon V, Blanchet D, Oger P, et al. Experiments and geochemical modelling of CO_2 sequestration by olivine: potential, quantification. Appl Geochem 2010;25:1383–96.
[29] Fischer S, Liebscher A, Wandrey M. CO_2–brine–rock interaction – first results of long-term exposure experiments at in situ P–T conditions of the Ketzin CO_2 reservoir. Chemie der Erde – Geochemistry 2010;70:155–64.
[30] Lin H, Fujii T, Takisawa R, Takahashi T, Hashida T. Experimental evaluation of interactions in supercritical CO_2/water/rock minerals system under geologic CO_2 sequestration conditions. J Mater Sci 2008;43:2307–15.
[31] McGrail BP, Schaef HT, Glezakou VA, Dang LX, Owen AT. Water reactivity in the liquid and supercritical CO_2 phase: has half the story been neglected? Energy Procedia 2009;1:3415–9.
[32] Kwak JH, Hu JZ, Hoyt DW, Sears JA, Wang CM, Rosso KM, et al. Metal carbonation of forsterite in supercritical CO_2 and H_2O using solid state ^{29}Si, ^{13}C NMR spectroscopy. J Phys Chem C 2010;114:4126–34.
[33] Kwak JH, Hu JZ, Turcu RVF, Rosso KM, Ilton ES, Wang C, et al. The role of H_2O in the carbonation of forsterite in supercritical CO_2. Int J Greenhouse Gas Control 2011;5:1081–92.
[34] Loring JS, Schaef HT, Turcu RVF, Thompson CJ, Miller QRS, Martin PF, et al. In situ molecular spectroscopic evidence for CO_2 intercalation into montmorillonite in supercritical carbon dioxide. Langmuir 2012;28:7125–8.
[35] Loring JS, Thompson CJ, Wang Z, Joly AG, Sklarew DS, Schaef HT, et al. In situ infrared spectroscopic study of forsterite carbonation in wet supercritical CO_2. Environ Sci Technol 2011;45:6204–10.
[36] Loring JS, Thompson CJ, Zhang C, Wang Z, Schaef HT, Rosso KM. In situ infrared spectroscopic study of brucite carbonation in dry to water-saturated supercritical carbon dioxide. J Phys Chem A 2012;116:4768–77.
[37] Yang NN, Yang XN. Molecular simulation of swelling and structure for Na-Wyoming montmorillonite in supercritical CO_2. Mol Simul 2011;37:1063–70.
[38] Ilton ES, Schaef HT, Qafoku O, Rosso KM, Felmy AR. In situ X-ray diffraction study of Na^+ saturated montmorillonite exposed to variably wet super critical CO_2. Environ Sci Technol 2012;46:4241–8.
[39] Schaef HT, Ilton ES, Qafoku O, Martin PF, Felmy AR, Rosso KM. In situ XRD study of Ca^{2+} saturated montmorillonite (STX-1) exposed to anhydrous and wet supercritical carbon dioxide. Int J Greenhouse Gas Control 2012;6:220–9.

[40] Schaef HT, Windisch CF, McGrail BP, Martin PF, Rosso KM. Brucite $Mg(OH_2)$ carbonation in wet supercritical CO_2: an in situ high pressure X-ray diffraction study. Geochim Cosmochim Acta 2011;75:7458–71.
[41] Regnault O, Lagneau V, Catalette H, Schneider H. Experimental study of pure mineral phases/supercritical CO_2 reactivity. Implications for geological CO_2 sequestration. C R Geosci 2005;337:1331–9.
[42] Takenouchi S, Kennedy GC. The binary system H_2O–CO_2 at high temperatures and pressures. Am J Sci 1964;262:1055–74.
[43] Gence N. Wetting behavior of magnesite and dolomite surfaces. Appl Surf Sci 2006;252:3744–50.
[44] Matyasik I, Leśniak G, Such P, Mikołajweski Z. Mixed wetted carbonate reservoir: origins of mixed wettability and affecting reservoir properties. Ann Societatis Geologorum Poloniae 2010;80:115–22.
[45] Sola BS, Rashidi F. Experimental study of hot water injection into low-permeability carbonate rocks. Energy Fuels 2008;22:2353–61.
[46] Strand S, Austad T, Puntervold T, Hognesen EJ, Olsen M, Barstad SMF. "Smart water" for oil recovery from fractured limestone: a preliminary study. Energy Fuels 2008;22:3126–33.
[47] RezaeiDoust A, Puntervold T, Strand S, Austad T. Smart water as wettability modifier in carbonate and sandstone: a discussion of similarities/differences in the chemical mechanisms. Energy Fuels 2009;23:4479–85.
[48] Gennes P-Gd, Brochard-Wyart F, Quéré D. Capillarity and wetting phenomena: drops bubbles pearls waves. New York (USA): Science + Business Media, Inc.; 2004.
[49] Radilla G, Kacem M, Lombard JM, Fourar M. Transport properties of Lavoux Limestone at various stages of CO_2-like acid–rock alteration. Oil Gas Sci Technol – Rev D IFP Energies Nouvelles 2010;65:557–63.
[50] Chiquet P, Broseta D, Thibeau S. Wettability alteration of caprock minerals by carbon dioxide. Geofluids 2007;7:112–22.
[51] Chiquet P, Daridon JL, Broseta D, Thibeau S. CO_2/water interfacial tensions under pressure and temperature conditions of CO_2 geological storage. Energy Convers Manage 2007;48:736–44.
[52] Behzadi H, Alvarado V. Impact of three-phase relative permeability model on recovery in mixed media: miscibility, IFT, and hysteresis issues. Energy Fuels 2010;24:5765–72.